A protease-mediated switch regulates the growth of magnetosome organelles in *Magnetospirillum magneticum*

Juan Wan[a], Patrick J. Browne[a], David M. Hershey[b], Elizabeth Montabana[c], Anthony T. Iavarone[d], Kenneth H. Downing[e,1], and Arash Komeili[a,2]

[a]Department of Plant & Microbial Biology, University of California, Berkeley, CA 94720; [b]Department of Bacteriology, University of Wisconsin–Madison, Madison, WI 53706; [c]Department of Structural Biology, Stanford University School of Medicine, Stanford, CA 94304; [d]QB3/Chemistry Mass Spectrometry Facility, University of California, Berkeley, CA 94720; and [e]Molecular Biophysics and Integrated Bioimaging Division, Lawrence Berkeley National Laboratory, Berkeley, CA 94720

Edited by Lia Addadi, Structural Biology, Weizmann Institute of Science, Rehovot, Israel; received June 24, 2021; accepted October 26, 2021

Magnetosomes are lipid-bound organelles that direct the biomineralization of magnetic nanoparticles in magnetotactic bacteria. Magnetosome membranes are not uniform in size and can grow in a biomineralization-dependent manner. However, the underlying mechanisms of magnetosome membrane growth regulation remain unclear. Using cryoelectron tomography, we systematically examined mutants with defects at various stages of magnetosome formation to identify factors involved in controlling membrane growth. We found that a conserved serine protease, MamE, plays a key role in magnetosome membrane growth regulation. When the protease activity of MamE is disrupted, magnetosome membrane growth is restricted, which, in turn, limits the size of the magnetite particles. Consistent with this finding, the upstream regulators of MamE protease activity, MamO and MamM, are also required for magnetosome membrane growth. We then used a combination of candidate and comparative proteomics approaches to identify Mms6 and MamD as two MamE substrates. Mms6 does not appear to participate in magnetosome membrane growth. However, in the absence of MamD, magnetosome membranes grow to a larger size than the wild type. Furthermore, when the cleavage of MamD by MamE protease is blocked, magnetosome membrane growth and biomineralization are severely inhibited, phenocopying the MamE protease-inactive mutant. We therefore propose that the growth of magnetosome membranes is controlled by a protease-mediated switch through processing of MamD. Overall, our work shows that, like many eukaryotic systems, bacteria control the growth and size of biominerals by manipulating the physical properties of intracellular organelles.

biomineralization | bacterial organelles | magnetosome | magnetotactic bacteria | magnetite

Biomineralization is a common phenomenon across the tree of life; one type is a biologically controlled mineral production process that is often initiated within intracellular membrane-bound organelles or vesicle-like structures (1, 2). For instance, matrix vesicles serve as initial sites for mineral formation in the growth plate and most other vertebrate mineralization tissues (3). Vesicles also play a central role in the formation of calcitic spicules in sea urchins (4), extracellular calcitic plates in marine coccolithophores (5), and the silica-based cell walls of diatoms (6). Compartmentalization within a membrane is believed to provide an isolated microenvironment and a template for efficient nucleation, growth, and shaping of minerals.

In contrast to the multiple examples of eukaryotic biomineralization noted here, little is known regarding the diversity and dynamics of bacterial biomineralization at the molecular and cellular level. Production of magnetic minerals within magnetosome organelles of magnetotactic bacteria (MTB) stands as one of the best-studied examples of biomineralization in bacteria. MTB are a diverse group of gram-negative bacteria often found near the oxic-anoxic transition zone of aquatic environments (7). Magnetic nanoparticles (magnetite or greigite) mineralized by MTB are generally 35 to 120 nm in length, a size range that yields a single, stable magnetic moment (8). Magnetosomes are typically arranged into one or multiple chains that function as a complete magnetic unit, enabling MTB to navigate along geomagnetic field lines and efficiently find the oxic-anoxic transition zone in a process termed magneto-aerotaxis (9).

Biomineralization compartments generally contain a specific cohort of proteins that play critical roles during organelle formation and mineralization. Proteins involved in magnetosome biogenesis are normally encoded from a genomic region called the magnetosome gene island (MAI) (*SI Appendix*, Fig. S1*A*). Many magnetosome-associated membrane (Mam) and magnetic particle membrane-specific (Mms) proteins are associated with magnetosomes (10–12). The genes encoding the Mam and Mms proteins are organized into four clusters (*mamAB*, *mamGFDC*, *mms6*, and *mamXY*) in the model *Magnetosprillum* species and are necessary and sufficient for magnetosome formation (13–17) (Fig. 1*A*). Analyses of deletion mutants have been used to assign roles for individual genes in one of four distinct stages of magnetosome biogenesis in the model organism *Magnetospirillum magneticum* AMB-1 (AMB-1): 1) empty membrane invagination (*mamI*, *-L*, *-Q*, and *-B*), 2) chain

Significance

Biomineralization, the process by which elaborate three-dimensional structures are built out of organic and inorganic molecules, is central to health and survival of many organisms. In some magnetotactic bacteria, the growth of magnetosome membranes is closely correlated to the progression of mineral formation. However, the molecular mechanisms of such regulation are not clear. We show that the serine protease MamE links magnetosome membrane growth to the controlled production of magnetite nanoparticles through the processing of mineral-associated MamD protein. Our results indicate that membrane growth directly controls mineral growth and shed light on how an organelle's size can determine its physiological output. Manipulation of the MamE pathway may also open the door for control of nanoparticle size in future biotechnological applications.

Author contributions: J.W., P.J.B., K.H.D., and A.K. designed research; J.W., P.J.B., D.M.H., E.M., and A.T.I. performed research; J.W., P.J.B., A.T.I., and K.H.D. contributed new reagents/analytic tools; J.W., P.J.B., D.M.H., E.M., A.T.I., and A.K. analyzed data; and J.W. and A.K. wrote the paper.

The authors declare no competing interest.

This article is a PNAS Direct Submission.

[1]Deceased August 2, 2018.

[2]To whom correspondence may be addressed. Email: komeili@berkeley.edu.

This article contains supporting information online at http://www.pnas.org/lookup/suppl/doi:10.1073/pnas.2111745119/-/DCSupplemental.

Published February 2, 2022.

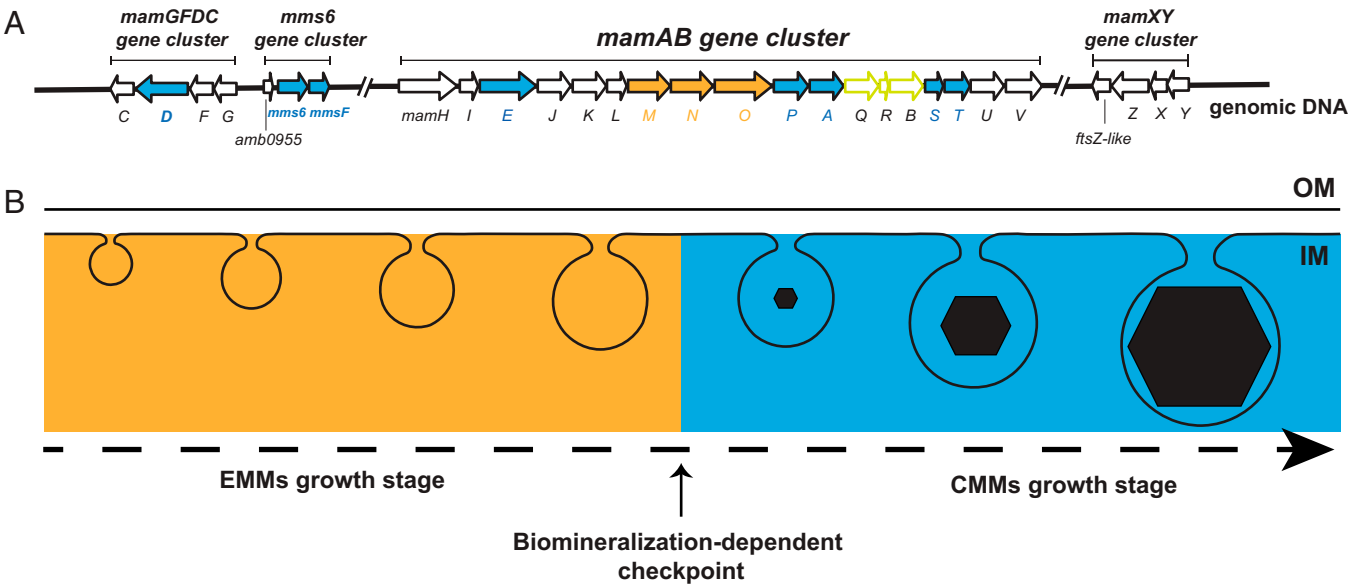

Fig. 1. The essential genes and the process of magnetosome production. (*A*) Schematic depicting the four key magnetosome gene clusters of AMB-1. A total of 10 genes were tested in this study for magnetosome membrane growth regulation: genes involved in crystal initiation (*mamM*, *-N*, and *-O*) are marked in orange, and genes involved in crystal maturation (*mamE*, *-P*, *-A*, *-S*, *-T*, *-D*, and *mms6*) are marked in blue. Based on previous work, *mmsF* is known to not be involved in magnetosome membrane growth (8). (*B*) Model of the biomineralization-dependent magnetosome membrane growth based on Cornejo et al. 2016 (19). OM, outer membrane. IM, inner membrane.

alignment (*mamK*, *-J,* and *-Y*), 3) crystal nucleation (*mamM*, *-N*, and *-O*), and 4) crystal maturation (other genes within the four clusters) (13, 14, 18) (Fig. 1*A*).

The resulting stepwise model outlines a set of processes that are seemingly distinct from one another. However, examination of the dynamics of magnetosome formation has revealed that magnetosome membrane growth is closely linked to the progression of biomineralization. Within a given AMB-1 cell, the magnetosome chain consists of some empty magnetosome membranes (EMMs) as well as the crystal-containing magnetosome membranes (CMMs) that provide the dipole moment necessary for orientation in magnetic fields. Cornejo et al. showed that at steady state, the diameter of the magnetosome lumen ranges from 20 to 80 nm (volume of about 4,189 to 268,083 nm^3), yet no EMMs grow beyond 55 nm (volume of about 65,450 nm^3) (19). Accordingly, when biomineralization is disrupted by limiting iron availability, only EMMs are produced and their growth stalls at about 55 nm, implying the existence of a checkpoint for membrane growth (Fig. 1*B*). Upon iron addition, membranes that have initiated biomineralization (CMMs) grow larger than this limit, implying that active biomineralization is needed for further membrane growth (19) leading to a linear relationship between the size of the growing crystals and the surrounding membranes (Fig. 1*B*). One possible explanation for these observations is that the growing mineral pushes against the membrane and drives its expansion. However, a mutant missing MmsF, a late-stage biomineralization protein, makes small magnetite crystals and still produces membranes as large as the wild-type (WT) parent in a biomineralization-dependent manner (19). These observations imply that magnetosome membrane growth is tightly regulated to create an optimal environment for crystal nucleation, which triggers the second membrane growth stage for crystal maturation (19).

The discovery of biomineralization-dependent magnetosome membrane growth provides a lens to examine the function of magnetosome proteins. One hypothesis holds that regulated growth of the magnetosome membrane allows for proper accumulation of iron to high concentrations to initiate nucleation and growth of magnetic particles. Thus, factors known to influence the growth and geometry of magnetite crystals may actually do so by regulating the physical properties of the magnetosome membrane. Here, we explored this possibility by using whole cell cryoelectron tomography (cryo-ET) to directly measure the sizes of magnetosome membranes in a series of mutants with known defects in crystal production. MamE belongs to a highly conserved high temperature requirement A (HtrA) family of trypsin-like serine proteases, whose activity is required for crystal maturation with an unknown mechanism (20). Here, we find that the catalytic activity of MamE plays a central role in the progression of magnetosome membrane growth. MamE proteolytically processes itself and two other biomineralization factors, MamO and MamP (21). MamO is required for MamE protease activation (22), and we find it acts as an upstream regulator of MamE for magnetosome membrane growth. MamP is not involved in magnetosome membrane growth. We also identified MamD, a protein that binds tightly to magnetite and was previously thought to promote crystal maturation (23, 24), as a direct substrate of MamE and showed that MamD is in fact a negative regulator of biomineralization. Our results indicate that MamE activates membrane remodeling by relieving MamD's inhibition on the size of the magnetosome lumen and demonstrate how spatial restructuring of an organelle can regulate its biochemical output.

Results

MamE Protease Activity Activates Magnetosome Membrane Growth. The *mamAB* gene cluster is the most important genetic unit for magnetosome biogenesis (25). Given the potential link between organelle size and biomineralization, we examined mutations that disrupt crystal nucleation (*mamM*, *-N*, and *-O*) or dramatically influence crystal maturation (*mamE*, *-P*, *-A*, *-S*, and *-T*) in the *mamAB* gene cluster (Fig. 1*A*). The first candidate is MamE. The MAI of AMB-1 has been separated into 14 different regions based on predicted operons (13) (*SI Appendix*, Fig. S1*A*). The *mamAB* gene cluster is in region 5 (R5), and region 9 (R9) contains an operon that encodes a few homologous

genes of the *mamAB* gene cluster, including an *mamE* homolog called *limE* (20) (*SI Appendix*, Fig. S1*A*). In the Δ*mamE*Δ*limE* strain containing a catalytically inactive MamE (protease dead *mamE*, $mamE^{pd}$) as the sole version of the protein (*SI Appendix*, Fig. S1 *A* and *B*), crystal nucleation and initial growth are indistinguishable from WT cells (20). However, further maturation of the crystals beyond 25 to 30 nm in size is severely inhibited (20).

We hypothesized that MamE protease activity is either required for direct biomineralization of magnetite or promotes biomineralization indirectly by activating magnetosome membrane growth. We used cryo-ET to determine the diameter of magnetosome membranes in WT AMB-1, the $mamE^{pd}$ mutant, and the complemented strain, $mamE^{wt}$. Consistent with previous observations (26), a single magnetosome chain with EMMs located between CMMs was detected in all three strains (Fig. 2 *A* and *B*, *SI Appendix*, Fig. S1*C*, and Movies S1–S3). As expected, the $mamE^{pd}$ mutant produces immature crystals, while $mamE^{wt}$ makes WT-like crystals. The size distribution of CMMs, as well as the linear relationship between crystals and the surrounding membranes, in $mamE^{wt}$ are similar to those in WT (Fig. 2*E*, *SI Appendix*, Fig. S1 *E* and *F*, and Table 1). In contrast, the diameters of EMMs and CMMs in $mamE^{pd}$ are both significantly smaller than those in WT (Fig. 2*E* and Table 1). A linear relationship between the size of crystals and the surrounding membranes in $mamE^{pd}$ still exists (*SI Appendix*, Fig. S1*G*). However, most CMMs in $mamE^{pd}$ are smaller than 55 nm in diameter, and the resident crystals are smaller than 25 to 30 nm in length (*SI Appendix*, Fig. S1*G*). Additionally, the linear regression line and the linear equation of $mamE^{pd}$ are a bit different from WT and $mamE^{wt}$ strains (*SI Appendix*, Fig. S1 *E*–*G*). This is likely due to different relationships between crystal size and membrane size in the two stages of magnetosome growth. In the first stage, biomineralization can lag relative to membrane growth, since EMMs grow to 55 nm prior to the initiation of crystal formation. In the second stage, membrane and crystal growth are coordinated. Since $mamE^{pd}$ magnetosomes are mostly in the first growth phase, a poorer linear relationship between membranes and crystals is observed. These results stand in contrast to our previous work on the major magnetite biomineralization regulator MmsF (19). In Δ*mmsF*, membranes of magnetosomes that harbor small crystals can grow as large as magnetosomes in the WT that harbor mature crystals (19). In other words, continued growth of a crystal is not a requirement for physical expansion of the magnetosome membrane. Hence, we conclude that the $mamE^{pd}$ biomineralization defect is likely due to a failure to expand the magnetosome membrane rather than direct control of crystal growth.

MamO and MamM Control the Protease Activity of MamE to Regulate Magnetosome Membrane Growth. To verify the role of MamE protease in magnetosome membrane growth, we examined mutants that disrupt the regulation of its catalytic activity. MamO is a bifunctional protein with separate roles in crystal nucleation and activation of MamE protease (22). We performed cryo-ET on Δ*mamO*ΔR9, a strain that removes the functionally redundant *limO* from the R9 region of the MAI (*SI Appendix*, Fig. S1*A*). Consistent with previous findings (13), Δ*mamO*ΔR9 produces a chain of EMMs across the cell (Fig. 2*C* and Movie S4) due to its essential role in crystal nucleation. The EMMs in Δ*mamO*ΔR9 are significantly smaller than those in WT but similar to those in $mamE^{pd}$ (Fig. 2*E*). As a control, we also imaged ΔR9 cells with cryo-ET. The size distributions of EMMs and CMMs in ΔR9 are similar to those in WT (*SI Appendix*, Fig. S2 and Movie S5). These findings further confirm the importance of an active MamE protease for magnetosome membrane growth.

MamM is a predicted iron transporter that is required for stable accumulation of MamB and regulation of iron flux to the magnetosome during crystal nucleation (27). We find that Δ*mamM* produces only empty magnetosomes (Fig. 2*D* and Movie S6), and 6 out of 12 Δ*mamM* cells we analyzed contained a very short magnetosome chain with about 5 EMMs. Surprisingly, the EMMs in Δ*mamM* are significantly smaller than those in WT but are similar to those in $mamE^{pd}$ (Fig. 2*E*). The similar size distribution of EMMs in $mamE^{pd}$, Δ*mamO*Δ*R9*, and Δ*mamM* prompted us to investigate if the MamE protease is functional in the Δ*mamM* background. MamE proteolytically processes itself in WT AMB-1 (21). Consistent with previous observations (22), immunoblotting with anti-MamE serum revealed full-length MamE and two processed forms in WT AMB-1 (Fig. 2*F*). In contrast, only full-length MamE was detected in Δ*mamO*Δ*R9* and $mamE^{pd}$ strains, confirming a defect in protease activity in these strains (Fig. 2*F*). Similarly, MamE is primarily found in its full-length form in the Δ*mamM* mutant (Fig. 2*F*). The signals for full-length MamE, normalized to total cellular protein, are enhanced 1.5- to 3-fold in $mamE^{pd}$, Δ*mamO*Δ*R9*, and Δ*mamM* strains as compared to the WT (*SI Appendix*, Fig. S3). Thus, in addition to MamO, MamM could be another activator of the MamE protease.

To summarize, when MamE protease activity is inhibited ($mamE^{pd}$, Δ*mamO*Δ*R9*, and Δ*mamM*), magnetosome membranes are significantly smaller than those in WT. Therefore, MamE and the proper regulation of its protease activity are crucial for magnetosome membrane growth.

Discovering MamE Proteolytic Targets that Affect Magnetosome Membrane Growth. Based on the results above, we hypothesized that MamE protease controls magnetosome membrane size by proteolytic removal of one or more inhibitors. We would predict that an uncleavable version of such an inhibitor would result in small magnetosome membranes while its loss would yield magnetosome membranes larger than those of the WT strain. In addition to MamO and MamE, MamP is the only other known substrate of MamE (21). Since MamO acts upstream of MamE, we asked if MamP could be the downstream membrane growth inhibitor. Although the percentage of EMMs in Δ*mamP* (~60%) is about twice as much as in WT (~35%) (Table 1), the size distribution of EMMs in Δ*mamP* was similar to those in WT (*SI Appendix*, Fig. S2 and Movie S7). Similar to previous observations (13), most of the crystals in Δ*mamP* cells are smaller than those of WT, while a few crystals in each Δ*mamP* cell are even larger than the mature crystals in WT. Despite these biomineralization anomalies, statistical analysis showed that the CMMs in Δ*mamP* were significantly smaller than those in WT (*SI Appendix*, Fig. S2), which indicates that MamP is not an inhibitor for magnetosome membrane growth.

Using a candidate approach surveying magnetosome proteins, we discovered that Mms6 may be a potential target of MamE protease (*SI Appendix*, Fig. S4 *A* and *B*). Immunoblotting against GFP shows that full-length Mms6-GFP and multiple processed bands can be seen in WT (*SI Appendix*, Fig. S4*B*). However, only full-length Mms6-GFP is detected in $mamE^{pd}$ and Δ*mamE*Δ*limE* strains (*SI Appendix*, Fig. S4*B*). Mms6 is encoded by the *mms6* gene cluster (Fig. 1*A*) and has been shown to play roles in crystal size and shape regulation (28). To test if Mms6 is a membrane growth inhibitor, we imaged the Δ*mms6* mutant with cryo-ET (*SI Appendix*, Fig. S4*C*). Although the sizes of crystals in Δ*mms6* are significantly smaller than those in WT (*SI Appendix*, Fig. S4*D*), the sizes of EMMs and CMMs are similar between the Δ*mms6* and the WT strains (*SI Appendix*, Fig. S4*E*). Thus, to this point, all known MamE substrates either regulate

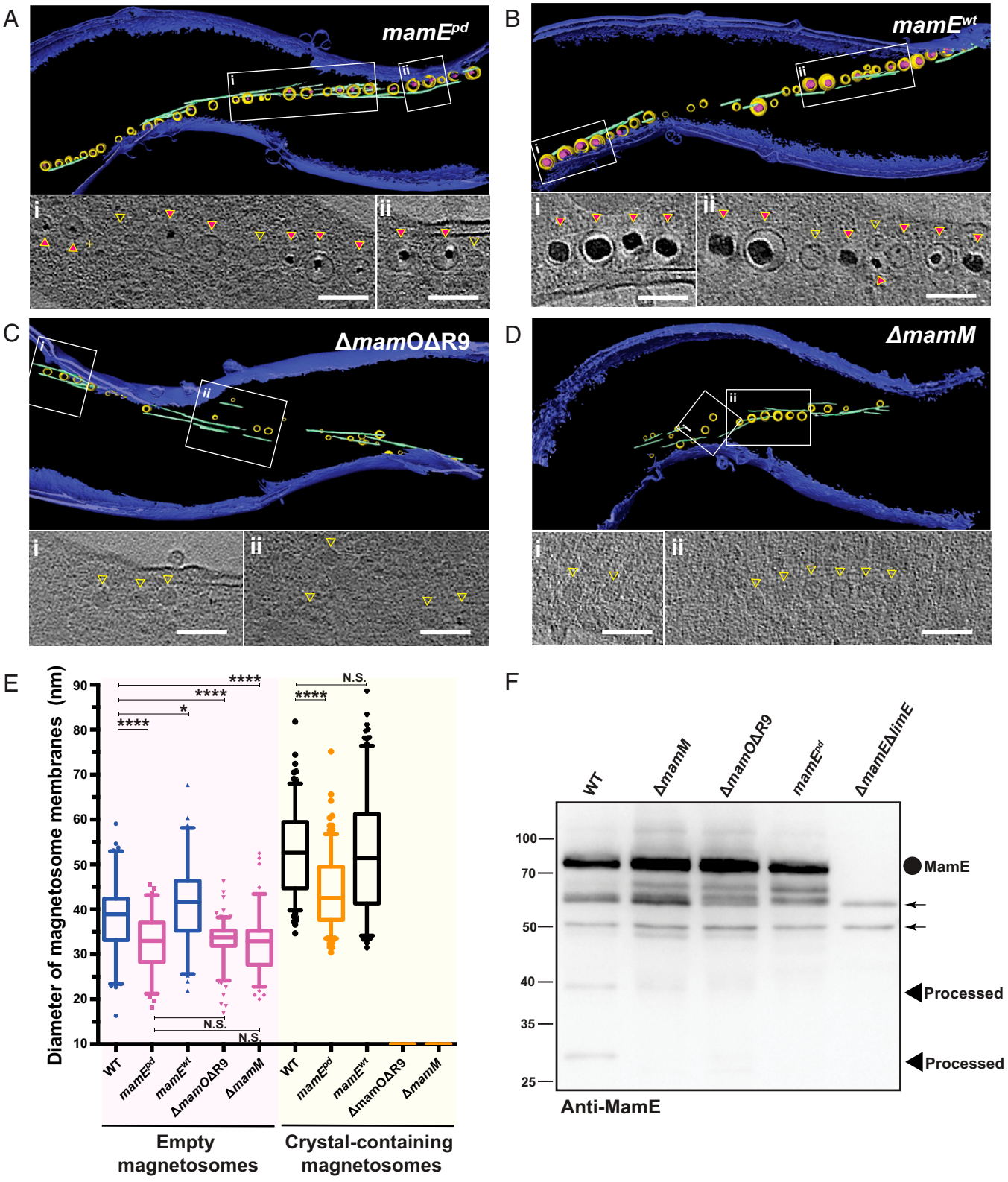

Fig. 2. MamE plays a key role in magnetosome membrane growth. (*A–D*) Segmented three-dimensional models (*Upper*) and selected area of tomographic slices (*Lower*, boxes i and ii) showing representative phenotypes of *mamE*^{pd} (*A*), *mamE*^{wt} (*B*), Δ*mamO*ΔR9 (*C*), and Δ*mamM* (*D*) strains. Here and below: The outer and inner cell membranes are depicted in blue, magnetosome membranes in yellow, magnetic particles in magenta, and magnetosome-associated filaments in green. Empty yellow arrowheads point to EMMs, and yellow arrowheads filled with magenta point to CMMs on tomographic slices. (Scale bars, 100 nm.) Full tomograms are shown in Movies S2–S4 and S6. (*E*) Diameters of EMMs and CMMs were measured from cryoelectron tomograms of WT, *mamE*^{pd}, *mamE*^{wt}, Δ*mamO*ΔR9, and Δ*mamM* strains. Here and below: The box plots show the median (line within box), the first and third quartiles (*Bottom* and *Top* of box), and 5 to 95 percentile (whiskers). Points below and above the whiskers are drawn as individual points. *P* values were calculated by *t* tests or Mann–Whitney *U* tests. No statistically significant difference ($P > 0.05$, N.S.), significant difference (*$P < 0.05$, ****$P < 10^{-4}$). (*F*) Immunoblotting analysis of MamE autoprocessing within the indicated genetic backgrounds. Full-length MamE proteins (~75 kDa) are marked with a circle, and proteolytic fragments (one is about 40 kDa and another one is about 30 kDa) are marked with arrowheads. Nonspecific bands are denoted by arrows and used as loading control.

Table 1. Measurements of magnetosome membrane size for various AMB-1 strains

Figures	Strain	Diameters of EMMs median/ (mean ± SD) (nm)	Surface area of EMMs (nm^2)	Diameters of CMMs median/ (mean ± SD) (nm)	Surface area of CMMs (nm^2)	Number of EMMs/CMMs	% of EMMs	Number of cells measured
Figs. 2*E* and 5*D* and *SI Appendix*, Figs. S2, S4*E*, S6*C*	WT AMB-1	38.9/(38.2 ± 7.8)	4,753.9	52.6/(52.6 ± 9.1)	8,692.0	84/158	34.7%	13
Figs. 2*E* and 5*D*	*mamE*^{pd}	33.0/(32.6 ± 6.1)	3,421.2	42.6/(44.0 ± 7.7)	5,701.2	67/191	30%	9
Fig. 2*E*	*mamE*^{wt}	41.6/(41.3 ± 8.8)	5,436.7	51.4/(52.6 ± 13.0)	8,300.0	67/191	30%	6
	Δ*mamO*ΔR9	33.8/(33.1 ± 4.1)	3,589.1	—	—	163/-	100%	9
	Δ*mamM*	32.9/(32.4 ± 6.2)	3,400.5	—	—	96/-	100%	12
SI Appendix, Fig. S2	ΔR9	40.7/(39.5 ± 5.9)	5,204.0	53.2/(54.3 ± 8.5)	8,891.5	43/102	30%	7
	Δ*mamP*	41.4/(40.7 ± 9.4)	5,384.6	46.0/(47.9 ± 12.8)	6,647.6	71/47	60.2%	5
	Δ*mamA*	38.7/(40.8 ± 8.9)	4,705.1	54.2/(55.8 ± 10.6)	9,228.9	182/96	65.5%	14
	Δ*mamS*	43.0/(44.2 ± 8.4)	5,808.8	54.5/(54.5 ± 7.4)	9,331.3	60/56	51.7%	6
	Δ*mamT*ΔR9	41.0/ (41.8 ± 9.3)	5,281.0	56.3/(56.0 ± 6.8)	9,957.9	94/183	33.9%	12
	Δ*mamN*	38.6/(41.3 ± 13.3)	4,680.9	—	—	232/-	100%	8
Fig. 5*D*	WT/FLAG-MamD	30.5/(31.2 ± 7.3)	2,922.5	42.0/(42.1 ± 6.9)	5,541.8	172/42	80.4%	7
SI Appendix, Fig. S4*E*	Δ*mms6*	39.1/ (39.3 ± 10.2)	4,802.9	53.1/ (52.6 ± 7.2)	8,858.1	33/136	19.5%	7
SI Appendix, Fig. S6*C*	Δ*mamD*	41.6/ (41.4 ± 7.8)	5,436.7	55.1/(56.2 ± 9.1)	9,537.9	86/193	30.8%	9

The surface area of EMMs and CMMs were calculated based on the median value of the diameters using the equation of $A = 4\pi r^2$. r, radius. —, not applicable.

its activity, leading to an inhibition of membrane growth or do not participate in magnetosome membrane size regulation.

All known MamE substrates to date, including Mms6 described here, have been identified through a candidate approach by comparing their proteolytic processing in WT and MamE protease mutant backgrounds using immunoblotting (21). To identify additional proteolytic targets of MamE, we developed an unbiased, proteomic approach. Proteases are enzymes that hydrolyze proteins into smaller polypeptides or single amino acids. Inhibition of protease activity would stop the cleavage event, which may result in an increased abundance of targeted proteins. We hypothesized that the concentrations of MamE-targeted proteins would be elevated in the magnetosomes of the *mamE*^{pd} mutant relative to the WT background. Thus, we isolated magnetosomes from both *mamE*^{wt} and *mamE*^{pd} and analyzed protein composition with liquid chromatography-mass spectrometry (LC-MS). To reduce background contamination from cellular proteins and increase specificity, we developed a process to enrich magnetosomes with their membranes intact but separate from bacteria inner membrane and cytoplasmic fractions (*SI Appendix*, Fig. S5*A*). After analysis by LC-MS, 28 proteins showed a 20-fold or higher enrichment in isolated magnetosomes from *mamE*^{wt} (*SI Appendix*, Table S1) when ranked by enrichment over their abundance in the lysate fraction and filtered for having a sufficient number of peptides (*SI Appendix, SI Materials and Methods*). A total of 19 of the 28 enriched proteins are encoded by the MAI or magnetotaxis islet (MIS) and have been suggested to be involved in magnetosome production (*SI Appendix*, Table S1). We then compared the proteomic profiles of magnetosomes isolated from *mamE*^{wt} to those from *mamE*^{pd}. As a validation of this approach, we found that the amount of MamE in magnetosomes from *mamE*^{pd} shows a 1.7-fold increase compared to *mamE*^{wt} (Fig. 3*A*), which is consistent with the immunoblotting quantification data (*SI Appendix*, Fig. S3*B*). Most other magnetosome proteins showed similar abundances in the magnetosomes of both strains as exemplified by MamA in Fig. 3*A*. In contrast, one magnetosome protein, MamD (also known as Mms7), and three proteins (Amb3286, Amb3288, and Amb3289) encoded by a putative operon outside of MAI were greatly enriched in magnetosomes from *mamE*^{pd} (Fig. 3*A*). Amb3286, Amb3288, and Amb3289 are annotated as tetrathionate reductase subunits A, C, and B, respectively. Our initial investigation of their mutant phenotypes indicates that they are not involved in magnetosome formation. Thus, we chose to focus on *mamD,* a gene found within one of the four MAI gene clusters essential and sufficient for magnetosome biosynthesis (16).

MamD (~30 kDa) is encoded by the *mamGFDC* gene cluster (Fig. 1*A*) and is predicted to contain a single carboxyl-terminal transmembrane helix and a larger amino-terminal region that localizes to the magnetosome lumen (Fig. 3*C*). Indeed, fragments of MamD have been identified in other analyses of magnetosome-associated proteins (10, 24). An amino-terminal 22-kDa MamD fragment was detected on purified magnetosomes from *Magnetospirillum gryphiswaldense* MSR-1 (MSR-1) (10). A carboxyl-terminal 7-kDa MamD fragment was detected when searching for magnetosome proteins that bound tightly to the magnetite crystals in AMB-1 (24). The MamD proteins from AMB-1 and MSR-1 have an 85% identity with the same number of amino acids. The proteomic analyses suggest the presence of two potential fragments of MamD and maybe at least two cleavage sites on MamD (between aa_{229} and aa_{259}) (Fig. 3*C*). To test if MamE targets MamD in vivo, we used immunoblotting to compare MamD processing in WT and mutants with disrupted MamE protease activity. As expected, a full-length MamD and a processed form are present in WT (Fig. 3*B*). The size of the processed MamD is similar to the long amino-terminal fragment detected via proteomics in MSR-1. A shorter fragment corresponding to the carboxyl terminus was not detected, likely because antibodies were raised against the soluble amino-terminal section of MamD (aa_1 through aa_{270}). Full-length MamD is more abundant in Δ*mamE*Δ*limE*, and no processed MamD was detected in this background (Fig. 3*B*). For the three mutants (Δ*mamM*, Δ*mamO*Δ*R9*, and *mamE*^{pd}) that contain an inactivated MamE protease, only full-length MamD but not the

MICROBIOLOGY

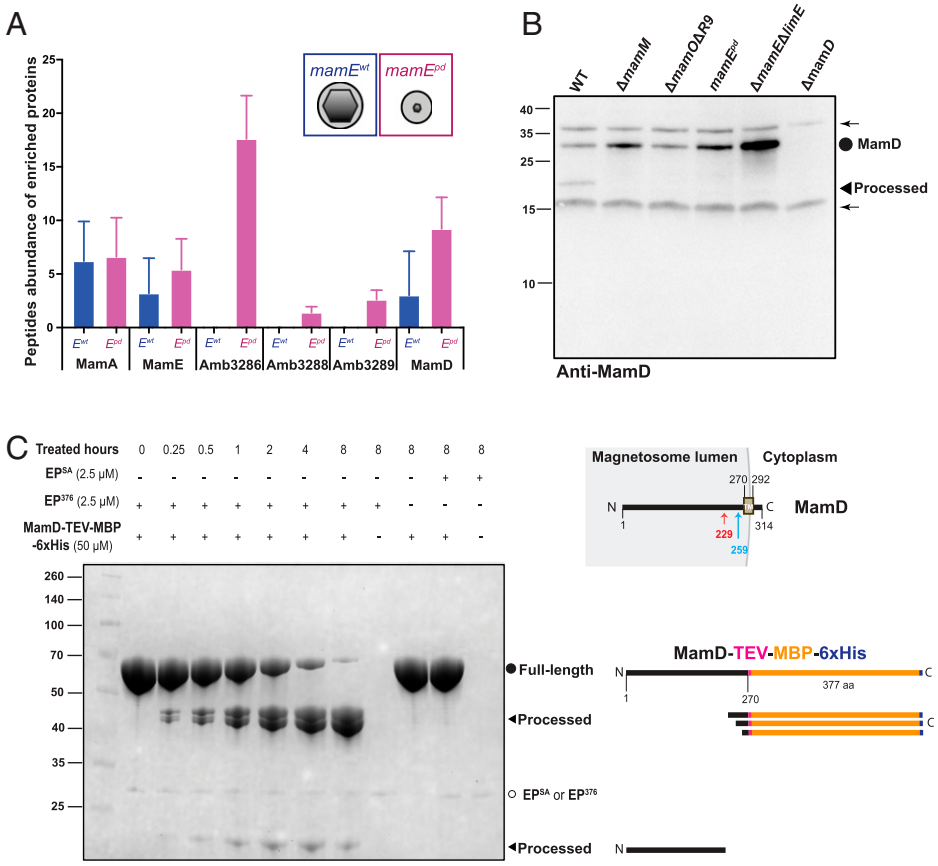

Fig. 3. MamE protease cleaves MamD. (*A*) A comparison of peptide counts mapped to representative proteins that are associated with magnetosomes isolated from *mamE*^{wt} and *mamE*^{pd} strains. MamA shows no noticeable differences between the two strains. MamE is slightly enriched, while Amb3286, Amb3288, Amb3289, and MamD are clearly enriched in purified magnetosomes from *mamE*^{pd}. The mean values of peptides for each protein are from five distinct preparations of magnetosomes (see full dataset in Dataset S1). (*B*) Immunoblotting analysis of MamE-dependent processing MamD in vivo. Full-length MamD (~30 kDa) is marked with a circle, and proteolytic fragments (~22 kDa) are marked with an arrowhead. Nonspecific bands are indicated by arrows and used as loading controls. (*C*) SDS-PAGE analysis of an 8-h in vitro incubation of purified MamD-TEV-MBP-6xHis incubated with purified active MamE protease domain (EP^{376}) or inactive protease domain (EP^{SA}). On the top right is a predicted secondary structure of MamD including an amino-terminal region (aa$_1$ through aa$_{270}$), a transmembrane domain (aa$_{270}$ through aa$_{292}$), and a carboxyl-terminal region (aa$_{292}$ through aa$_{314}$). The red and blue arrows indicate the possible cleavage sites based on the sizes of detected MamD fragments. Note that the larger processed bands appear in triplets (as shown by the diagram on the right), indicating more than two possible cleavage sites on MamD.

processed MamD forms were detected (Fig. 3*B*). Therefore, it is likely that MamD is cleaved by MamE in vivo.

To confirm that MamE cleaves MamD directly, the soluble portion of MamD (aa$_1$ through aa$_{270}$, ~25 kDa) was fused to a TEV-MBP-6xHis (~43 kDa) tag and purified from *Escherichia coli* (Fig. 3*C*). When incubated with purified MamE protease domain (EP^{376}), the fusion protein MamD-TEV-MBP-6xHis is cleaved into three similarly sized larger bands (~45 kDa) and one smaller band (~22 kDa) over time (Fig. 3*C*), indicating multiple processing sites on MamD. The amount of MamD cleaved is dependent on time and the concentration of the MamE protease in the reaction (Fig. 3*C* and *SI Appendix*, Fig. S5*B*). A catalytically inactive variant of the MamE protease domain (EP^{SA}) does not cleave MamD-TEV-MBP-6xHis (Fig. 3*C* and *SI Appendix*, Fig. S5*C*). The larger processed bands react with anti-MamD, anti-MBP tag, and anti-6xHis tag antibodies, but the smaller processed band reacts only with anti-MamD antibodies (*SI Appendix*, Fig. S5*D*). Based on these results, we suggest that MamD is first processed by MamE protease into two fragments followed by two more processing events of the carboxyl-terminal fragment with all cleavage sites close to aa$_{229}$ through aa$_{259}$ (Fig. 3*C*). Further attempts to pinpoint the exact cleavage sites on MamD via LC-MS proved unsuccessful.

MamD Controls Magnetosome Membrane Growth. To examine if MamD regulates magnetosome membrane growth, we generated a Δ*mamD* strain. Coefficient of magnetism (Cmag) is a differential light-scattering method that quantifies the ability of MTB to orient in an external magnetic field (29) and correlates well to the biomineralization capability of MTB. The bulk magnetic response Cmag of the Δ*mamD* stain was only slightly lower than that of WT (Fig. 4*A* and Table 2). Analysis of conventional transmission electron microscopy (TEM) images showed that the number and size of crystals in Δ*mamD* are both slightly but not significantly smaller than those in WT (Fig. 4 *B* and *C* and Table 2). Furthermore, the crystal size distribution is similar between WT and Δ*mamD* (Fig. 4*D*). To measure the sizes of magnetosome membranes, we also imaged the Δ*mamD* mutant with cryo-ET (*SI Appendix*, Fig. S6*A*). Consistently, the size of crystals in Δ*mamD* was slightly but not significantly smaller than in the WT (*SI Appendix*, Fig. S6*B*). However, the sizes of EMMs and CMMs were both significantly larger than those in WT (*SI Appendix*, Fig. S6*C*), indicating that MamD inhibits magnetosome membrane growth.

The increase in magnetosome membrane size in the absence of *mamD* is consistent with its potential role as an inhibitor of membrane growth. In such a model, a block in processing of MamD, as seen in the absence of MamE activity, should inhibit

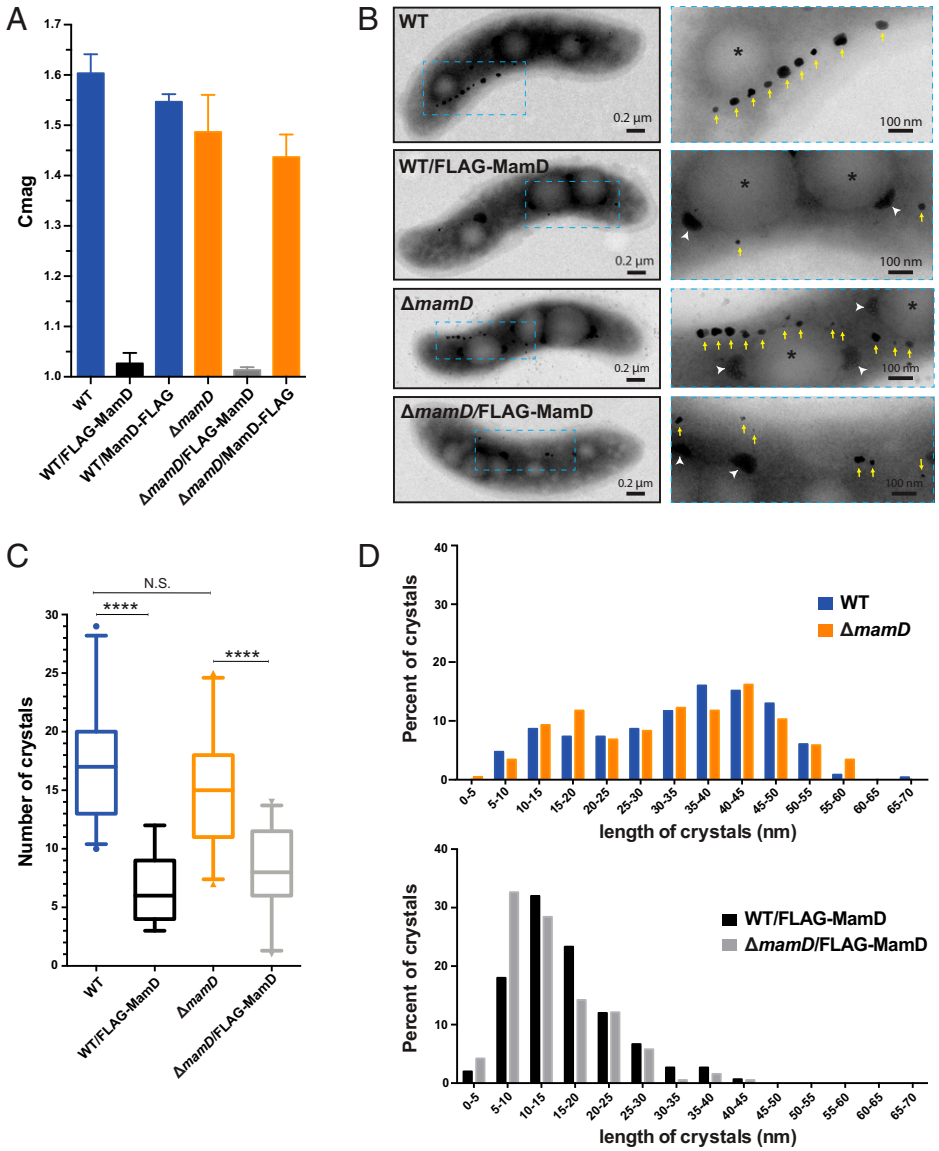

Fig. 4. Amino-terminally FLAG-tagged MamD severely hinders biomineralization. (*A*) Magnetic response (Cmag) of WT and Δ*mamD* cultures with or without FLAG-MamD and MamD-FLAG–expressing plasmids. WT and Δ*mamD* strains containing FLAG-MamD have minimal Cmag. Each measurement represents the average and SD from three independently grown cultures. (*B*) TEM micrographs of WT, WT/FLAG-MamD, Δ*mamD*, and Δ*mamD*/FLAG-MamD cells. Yellow arrows point to the magnetic particles. Black asterisks mark the PHB granules. White arrowheads point to the polyphosphate granules. (*C*) Quantification of the crystal numbers in WT and different variant strains. No statistically significant difference ($P > 0.05$, N.S.), significant difference (****$P < 10^{-4}$). (*D*) Distribution of crystal size in WT and different variant strains.

magnetosome membrane growth. To draw a direct link between MamD processing and magnetosome membrane growth, we sought to generate an uncleavable version of the protein. First, we made deletion and point mutations across the potential cleavage region of MamD as estimated by the cleavage products mapped above, none of which yielded an uncleavable form of the protein. However, we serendipitously blocked processing of native MamD by MamE in the course of related experiments. While creating tagged versions of MamD, we discovered that expressing an amino-terminal-3xFLAG tag (FLAG-MamD) dramatically decreased the magnetic response of WT cells (Fig. 4*A* and Table 2). In contrast, the magnetic response of cultures expressing the carboxyl-terminally tagged protein (MamD-FLAG) is similar to those with an empty plasmid (Fig. 4*A*). Compared to WT cells, WT/FLAG-MamD cells produce smaller crystals, confirming that the altered magnetic response is due to a biomineralization defect (Fig. 4*B*). Furthermore, compared to WT, the number of crystals per cell is significantly decreased in the WT/FLAG-MamD strain (Fig. 4*C*). WT showed a bimodal crystal size distribution with peaks centered in the 10- to 15-nm and 35- to 40-nm size ranges (Fig. 4*D*). In comparison, the crystal size distribution of the WT/FLAG-MamD strain is only centered at 10 to 15 nm (Fig. 4*D*). Compared with Δ*mamD*, the number of crystals is also significantly decreased in the Δ*mamD*/FLAG-MamD strain (Fig. 4*C*) and its crystal size distribution is centered at 10 to 15 nm (Fig. 4*D*). Together, these results indicate that FLAG-MamD severely inhibits biomineralization in both WT and Δ*mamD* strains.

One concern is whether the 3xFLAG tag (DYKDHDG-DYKDHDI-DYKDDDDK) itself affects iron biomineralization in magnetosomes. We have previously fused 3xFLAG tag with the other magnetosome membrane proteins such as MamE, MamP, and MamO (21). MamO has multiple transmembrane domains, and, similar to MamD, MamE and MamP are predicted

Table 2. Measurements of magnetic response and crystal properties for various strains

Strain	Plasmid	Cmag	Average length (mean ± SD)	Average width (mean ± SD)	Average shape factor	Number of crystals measured
WT AMB-1	pAK605	1.60 ± 0.04	33.3 ± 13.2 nm	26.6 ± 11.0 nm	0.81 ± 0.11	231
WT/FLAG-MamD	pAK1061	1.03 ± 0.02	16.2 ± 7.5 nm	13.0 ± 6.9 nm	0.79 ± 0.13	150
Δ*mamD*	pAK605	1.49 ± 0.07	32.5 ± 13.6 nm	24.7 ± 10.6 nm	0.77 ± 0.13	204
Δ*mamD*/FLAG-MamD	pAK1061	1.01 ± 0.01	13.9 ± 7.3 nm	10.6 ± 5.4 nm	0.78 ± 0.12	190

Cmag, average crystal length and average crystal width of various strains were measured as detailed in experimental procedures. Shape factor is calculated as the width divided by the length.

to have one transmembrane domain. Both the N- or carboxyl-terminally tagged MamE and MamP complemented the biomineralization defects of their respective deletion mutants (note that the carboxyl terminus of these proteins is predicted to be within the magnetosome). Additionally, FLAG-MamO complements the biomineralization defect of Δ*mamO*. These results indicate that the 3xFLAG tag fusion generally does not affect the function of magnetosome membrane proteins and iron biomineralization but that FLAG-MamD is an exception.

The phenotype of crystal size distribution in WT/FLAG-MamD strain is similar to the one in *mamE*^{pd} (15). One possible explanation is that MamE protease activity in general is inhibited in WT and Δ*mamD* strains expressing FLAG-MamD. However, self-processing of MamE and cleavage of MamP are unaffected in strains expressing FLAG-MamD (Fig. 5*A*), indicating that MamE functions normally in the FLAG-MamD background despite the dramatic reduction in biomineralization. In contrast, immunoblotting analysis using anti-MamD antibodies showed that the native MamD is not cleaved in WT/FLAG-MamD strain but can still be processed in the WT/MamD-FLAG strain as in WT (Fig. 5 *A* and *B*). The FLAG-tagged MamD variants are not directly detected with the anti-MamD antibodies, since they overlap with a nonspecific band on the blot (Fig. 5*A*). However, detection using anti-FLAG antibodies shows that both variants are expressed in these experiments (*SI Appendix*, Fig. S7). Moreover, immunoblotting analysis using anti-FLAG antibodies showed that FLAG-MamD is still proteolytically processed in WT and Δ*mamD* strains (*SI Appendix*, Fig. S7 and *SI Results*). Since the processed FLAG-MamD signal is detectable with anti-FLAG antibodies but not the anti-MamD antibodies, we speculate that the expression level of FLAG-MamD is much lower than the native MamD. Together, these results indicate that expression of FLAG-MamD can dramatically reduce the cleavage of native MamD by MamE in trans.

To test if FLAG-MamD inhibits biomineralization through magnetosome membrane growth control, we imaged WT/FLAG-MamD strain with cryo-ET (Fig. 5*C* and Movie S8). Both EMMs and CMMs are significantly smaller in the WT/FLAG-MamD strain than those in WT but are similar to those in the *mamE*^{pd} strain (Fig. 5*D*). The majority of magnetosomes in the WT/FLAG-MamD strain are EMMs (~80%), which is more than two times as much as in WT (~35%). Altogether, these findings indicate that FLAG-MamD inhibits the cleavage of native MamD in a dominant-negative fashion. As a consequence, the growth of magnetosome membranes is inhibited, resulting in the production of very few small magnetite particles. These results draw a direct line between the regulation of MamE activity, its processing of MamD, and growth of magnetosome membranes.

Discussion

The membranes and the associated proteins of biomineralization organelles control the size, shape, and composition of biominerals. Yet how organelle size is dynamically manipulated during mineral production is unclear. Here, we describe a protease-mediated pathway (Fig. 5*E*) that regulates the size of the magnetite biomineralization organelle in MTB. HtrA family proteases are widely conserved in a variety of bacterial and eukaryotic cells in which they are involved in protein quality control, nondestructive protein processing, or modulation of signaling pathways (30). The protease activity of MamE had previously been linked to crystal maturation via an unknown mechanism (20). Our results show that MamE controls crystal growth indirectly via manipulation of magnetosome membrane size. Furthermore, we found that upstream regulators of MamE protease activity (MamO and MamM) and a downstream target (MamD) play essential roles in regulating magnetosome membrane growth (Fig. 5*E*).

The essential role of upstream activators MamO and MamM in magnetosome membrane growth regulation underscores the importance of a proper control of the MamE protease activity. The catalytic activity of HtrA family proteases is tightly regulated to protect cellular proteins from uncontrolled and unspecific proteolysis (31). The basal state of MamE protease is an inactive form, and the catalytic activity of MamE could be turned on through several different routes, including the presence of substrate and peptide binding to either of its PDZ domains (21). MamO is a known MamE protease activator, and the activation of MamE protease activity is controlled by MamO's carboxyl-terminal ion transporter domain (22). Here, we discovered MamM as another potential MamE protease activator. MamM belongs to the cation diffusion facilitator family that transports iron into the magnetosome lumen (27). Hence the accumulation or flux rate of iron, mediated by MamM, may be a signal to activate MamE. Alternatively, MamM might indirectly affect MamE protease activation by interacting with and stabilizing MamB, another putative cation transporter that is required for magnetosome membrane formation. Instability of MamB could be the reason for the observation of very few empty magnetosomes in the Δ*mamM* strain, since MamB was suggested to serve as a landmark protein that induces the formation of larger protein complexes for EMMs invagination (32).

We also find that MamE protease controls crystal production by proteolytically processing MamD. MamD was originally identified through its tight binding to the magnetite crystals within magnetosomes. Genetic experiments led to a model in which MamD acts as a promoter of biomineralization by controlling the size and shape of crystals (17, 23). Instead, we show that MamD is a magnetosome membrane growth inhibitor. Loss of MamD results in a size increase of magnetosome membranes, which only slightly affects crystal maturation. However, we find that expressing a FLAG-tagged MamD (FLAG-MamD) dramatically reduces the cleavage of native MamD by MamE protease, leading to a severe inhibition of magnetosome membrane growth and crystal maturation. Since FLAG-MamD does not disrupt the general enzymatic function of MamE, we favor a model in which it behaves as a dominant-negative

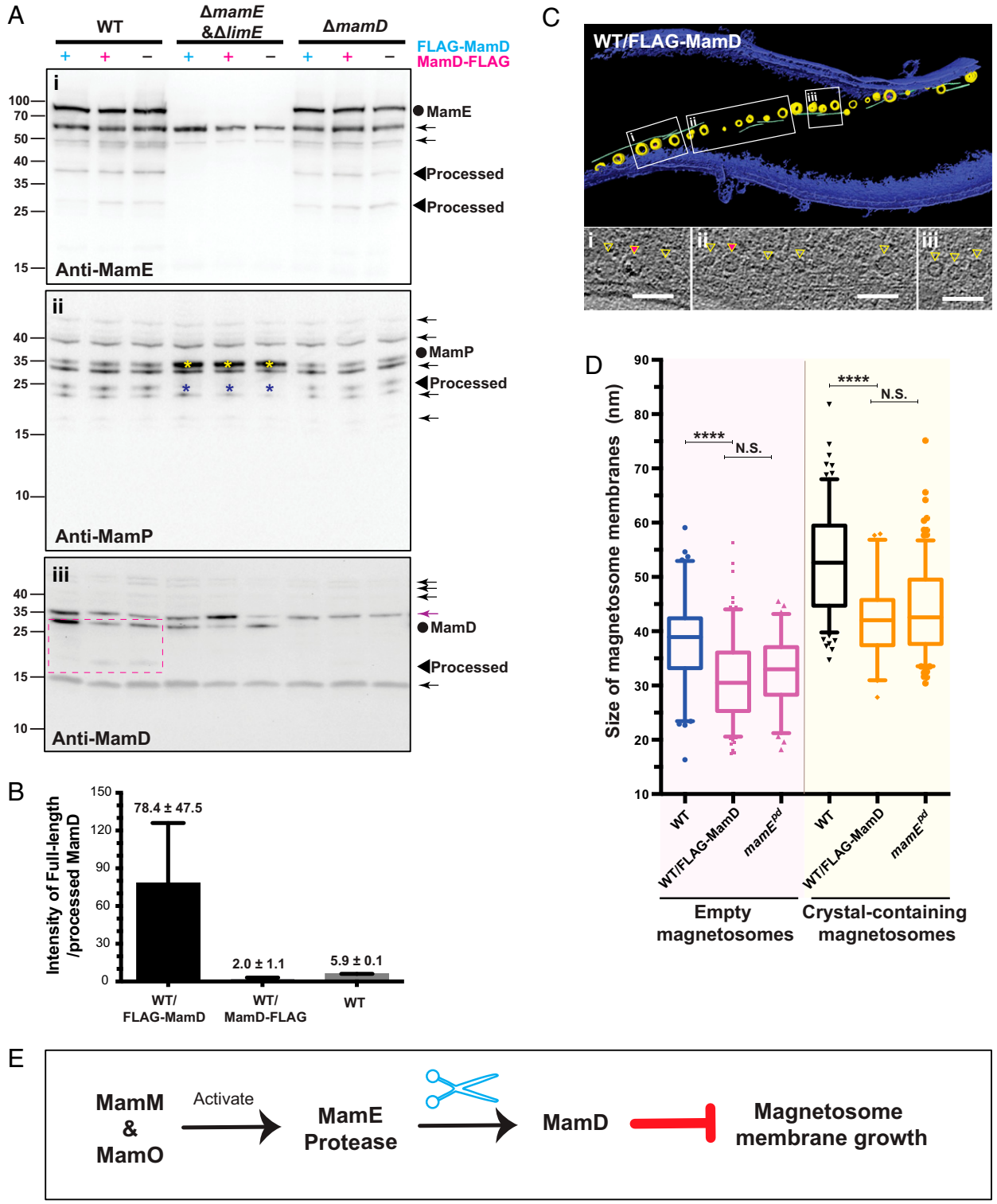

Fig. 5. FLAG-MamD blocks MamE processing of native MamD and inhibits magnetosome membrane growth. (*A*) Immunoblotting analysis of MamE processing itself (*i*), MamP (*ii*), and MamD (*iii*) within the indicated genetic backgrounds. Full-length proteins are marked with circles, and proteolytic fragments are marked with arrowheads. Nonspecific bands are indicated with arrows and used as loading controls. Yellow asterisks mark the enhanced full-length MamP (~35 kDa) bands, and blue asterisks mark the decreased processed MamP bands in Δ*mamE*Δ*limE* strains (*ii*). When using anti-MamD antibodies, the FLAG-MamD/MamD-FLAG are superimposed with a nonspecific band and show variable expression levels (purple arrow in *iii*). (*B*) The intensity ratio of full-length MamD versus processed MamD bands in WT background (dashed magenta rectangle in *A*, *iii*) were quantified. The experiment using anti-MamD antibodies was repeated three times, and the data were used to calculate the mean and SD. (*C*) A segmented three-dimensional model (*Upper*) shows representative phenotype of WT/FLAG-MamD strain. White boxes (*i–iii*) show the selected area of tomographic slices. (Scale bars, 100 nm.) Full tomograms are shown in Movie S8. WT/FLAG-MamD strain contains a magnetosome chain with mainly EMMs and a few CMMs across the cell axis. (*D*) Diameters of EMMs and CMMs were measured from cryoelectron tomograms of the WT/FLAG-MamD strain. No statistically significant difference ($P > 0.05$, N.S.), significant difference (****$P < 10^{-4}$). (*E*) Model of the MamE protease-mediated pathway for magnetosome membrane growth control.

mutant by inhibiting the cleavage of itself as well as native MamD. One possible explanation is that MamD assembles into a multimer that needs to be cleaved to allow for membrane expansion and promotion of magnetite growth. FLAG-MamD may incorporate itself into the multimer and alter the accessibility of MamE to the complex.

While our results clearly support a direct link between MamE and MamD in regulation of magnetosome membrane size, other MAI proteins may also participate in this process. AMB-1 contains a number of proteins in the same class as MamD, including a homolog (MamD-like) encoded from the MIS region. These proteins may perform overlapping functions with MamD in control of biomineralization and membrane growth. In support of this hypothesis, we find that FLAG-MamD also inhibits biomineralization in a Δ*mamD* strain. Additionally, in examining the membrane size distribution of several other mutants, we discovered that MamS, MamT, and MamN are also required for proper size regulation of magnetosome membranes. The EMMs in Δ*mamS* and Δ*mamT*ΔR9 are significantly larger than those in WT (*SI Appendix*, Fig. S2; see more details and the size distribution of CMMs in *SI Appendix, SI Results*). While the statistical analysis did not show a significantly different size distribution of EMMs in WT and Δ*mamN* (*SI Appendix*, Fig. S2), ∼18% of EMMs are larger than 55 nm in diameter in Δ*mamN*. These results indicate that the checkpoint for membrane growth might be circumvented in the absence of MamS, -T, or -N, resulting in larger EMMs. Whether MamS, -T, and -N act in parallel or link to the MamE-mediated magnetosome membrane growth regulation pathway will be explored in future experiments.

MamE protease is conserved in all sequenced MTB strains, indicating that MamE-mediated membrane size control could be broadly conserved in MTB. Indeed, our initial examination of the related model organism MSR-1 shows that there is a similar difference in size between EMMs and CMMs (*SI Appendix*, Fig. S9). Thus, we hypothesize that the MamE pathway also regulates membrane size in MSR-1 and, perhaps, in even more distantly related MTB. Given its diverse substrate profile, MamE is likely to impact steps of magnetosome formation distinct from membrane size regulation. Thus, studies using *mamE* deletion strains, or those expressing an inactive protease, are likely to impact multiple aspects of organelle assembly and biomineralization. By identifying an individual substrate and blocking its cleavage, we were able to isolate and examine one of the many possible functions of MamE. Moving forward, similar approaches targeting other MamE substrates can be effective in dissecting the many functions of this central regulator of magnetosome formation.

While our work highlights the important role of the MamE-mediated pathway for magnetosome membrane growth, the physical mode of magnetosome membrane expansion remains mysterious. Similar to previous observations (26), we also find that both the EMMs and CMMs are connected to the inner membrane of WT AMB-1 (*SI Appendix*, Fig. S1*D*), indicating that the magnetosome membranes could grow in size by addition of lipids and/or proteins from the connected inner membrane or directly from the cytoplasm. There is some evidence that protein transport to magnetosomes can be conditionally dependent on their biomineralization status. In particular, Mms6 is only associated with CMMs (33). Although *mms6* deletion does not affect magnetosome membrane growth, there might be other proteins that are added to magnetosomes at different growth stages to help increase the size of the magnetosome membranes. Moreover, the links between the stages of magnetosome membrane growth and their chemical composition remain unclear. We hypothesize that EMMs help to create optimal environment (iron concentration, pH, and redox state) for crystal nucleation. Perhaps membranes remain smaller to allow for more rapid increase in iron concentration to accelerate crystal nucleation.

A potential limitation of our findings is the small number of WT and mutant cells that could be studied (about 6 to 14 cells for each strain), since cryo-ET is a time- and resource-intensive methodology. However, we believe that our data are representative of the total population, since the crystal production phenotype from our cryo-ET is consistent with the other techniques, such as conventional TEM that sample hundreds or more cells.

Finally, our findings emphasize the importance of the cell biological features of intracellular organelles in biomineralization. We show that inhibiting or circumventing magnetosome membrane growth control severely impacts crystal production. Thus, in addition to creating a microenvironment for a specialized biochemical transformation, magnetosomes also promote mineral growth by actively manipulating organelle size. In the future, targeting the cell biological dimension of magnetosomes can lead to finer control over the size and magnetic properties of synthetic magnetic particles that can be used in biomedical and biotechnological applications.

Materials and Methods

Strains, Plasmids, and Bacterial Growth. The strains and plasmids used in this study are described in *SI Appendix*, Tables S2 and S3. The growth of AMB-1 and *E.coli* strains were as described previously (19) (*SI Appendix, SI Text*). The details of plasmid manipulation and deletion mutagenesis are described in *SI Appendix*.

TEM and Image Data Analysis. Cryo-ET imaging with AMB-1 strains was performed as described previously (19) with slight modification (*SI Appendix*). The diameter of magnetosome membranes was measured as described previously (19) (*SI Appendix*). Box plots of the membrane size distribution were generated by GraphPad Prism software (https://www.graphpad.com/scientific-software/prism/). Significant differences between two groups of samples were analyzed using *t* tests or the Mann–Whitney *U* test based on the normality of the analyzed datasets (*SI Appendix*). Conventional TEM was performed as described previously (13), and the details of crystal size quantification are described in *SI Appendix*.

Immunoblotting. Immunoblotting analysis was performed as described previously (21) with slight modifications (*SI Appendix*). Polyclonal antibodies to MamE and MamP have been described previously (22, 34). Polyclonal antibodies to MamD were raised by Covance in rabbits using a recombinant form of the amino-terminal section of MamD (aa_1 through aa_{270}). Polyclonal antibodies to MamT were raised by ProSci Inc. in rabbits against a synthetic peptide from the carboxyl terminus of MamT (CHDIVVKVPVDKKGGMRWQL) conjugated to a carrier protein. Monoclonal antibodies to Anti-MBP, Anti-6xHis, and anti-FLAG were purchased from commercial sources.

Magnetosome Isolation and Identification of Magnetosome-Associated Proteins. Magnetosomes were separated from $mamE^{wt}$ and $mamE^{pd}$ cells, and the magnetosome-associated proteins were analyzed with LC-MS (details in *SI Appendix*). The resulting proteins were ranked according to fold enrichment compared with cell lysate. Proteins that contained fewer than three tryptic peptides per 100 amino acids were removed. For magnetosomes from $mamE^{wt}$, all proteins remaining with a 20-fold or higher overabundance are listed in *SI Appendix*, Table S1.

Protein Expression, Purification, and In Vitro Proteolytic Analysis. The MamD-TEV-MBP-6xHis fusion protein, the MamE protease active domain (EP^{376}), and the MamE protease-inactive mutant domain (EP^{SA}) were expressed in BL21 Codon plus cells and purified using affinity purification (details in *SI Appendix*). Then, purified MamD-TEV-MBP-6xHis was mixed with either EP^{SA} or EP^{376}, and the protease-mediated cleavage was revealed by SDS-PAGE and Coomassie blue staining.

Data Availability. All study data are included in the article and/or supporting information.

ACKNOWLEDGMENTS. We thank Karen Davies for assistance with cryo-ET data processing using the cryo-EM facility at Lawrence Berkeley National Laboratory. We thank Daniel Toso for assistance with cryo-ET data collection and

Paul Tobias for computational support using the Berkeley Bay Area Cryo-EM Facility at University of California, Berkeley. We thank Brad Williams for assistance with the LC-MS data analysis from Waters Corporation. This work was funded by generous support from the NIH (R01GM084122 and R35GM127114). We thank members of the A.K. laboratory for helpful discussions and suggestions.

1. H. A. Lowenstam, Minerals formed by organisms. *Science* **211**, 1126–1131 (1981).
2. H. A. Lowenstam, S. Weiner, *On Biomineralization* (Oxford University Press, New York, 1989).
3. I. M. Shapiro, W. J. Landis, M. V. Risbud, Matrix vesicles: Are they anchored exosomes? *Bone* **79**, 29–36 (2015).
4. N. Vidavsky *et al.*, Initial stages of calcium uptake and mineral deposition in sea urchin embryos. *Proc. Natl. Acad. Sci. U.S.A.* **111**, 39–44 (2014).
5. A. R. Taylor, C. Brownlee, G. Wheeler, Coccolithophore cell biology: Chalking up progress. *Annu. Rev. Mar. Sci.* **9**, 283–310 (2017).
6. C. Heintze *et al.*, An intimate view into the silica deposition vesicles of diatoms. *BMC Materials* **2**, 11 (2020).
7. C. T. Lefèvre, D. A. Bazylinski, Ecology, diversity, and evolution of magnetotactic bacteria. *Microbiol. Mol. Biol. Rev.* **77**, 497–526 (2013).
8. D. A. Bazylinski, R. B. Frankel, Magnetosome formation in prokaryotes. *Nat. Rev. Microbiol.* **2**, 217–230 (2004).
9. C. T. Lefèvre *et al.*, Diversity of magneto-aerotactic behaviors and oxygen sensing mechanisms in cultured magnetotactic bacteria. *Biophys. J.* **107**, 527–538 (2014).
10. K. Grünberg, C. Wawer, B. M. Tebo, D. Schüler, A large gene cluster encoding several magnetosome proteins is conserved in different species of magnetotactic bacteria. *Appl. Environ. Microbiol.* **67**, 4573–4582 (2001).
11. K. Grünberg *et al.*, Biochemical and proteomic analysis of the magnetosome membrane in Magnetospirillum gryphiswaldense. *Appl. Environ. Microbiol.* **70**, 1040–1050 (2004).
12. M. Tanaka *et al.*, Origin of magnetosome membrane: Proteomic analysis of magnetosome membrane and comparison with cytoplasmic membrane. *Proteomics* **6**, 5234–5247 (2006).
13. D. Murat, A. Quinlan, H. Vali, A. Komeili, Comprehensive genetic dissection of the magnetosome gene island reveals the step-wise assembly of a prokaryotic organelle. *Proc. Natl. Acad. Sci. U.S.A.* **107**, 5593–5598 (2010).
14. D. Murat *et al.*, The magnetosome membrane protein, MmsF, is a major regulator of magnetite biomineralization in Magnetospirillum magneticum AMB-1. *Mol. Microbiol.* **85**, 684–699 (2012).
15. J. Yang *et al.*, MamX encoded by the mamXY operon is involved in control of magnetosome maturation in Magnetospirillum gryphiswaldense MSR-1. *BMC Microbiol.* **13**, 203 (2013).
16. I. Kolinko *et al.*, Biosynthesis of magnetic nanostructures in a foreign organism by transfer of bacterial magnetosome gene clusters. *Nat. Nanotechnol.* **9**, 193–197 (2014).
17. A. Scheffel, A. Gärdes, K. Grünberg, G. Wanner, D. Schüler, The major magnetosome proteins MamGFDC are not essential for magnetite biomineralization in Magnetospirillum gryphiswaldense but regulate the size of magnetosome crystals. *J. Bacteriol.* **190**, 377–386 (2008).
18. M. Toro-Nahuelpan *et al.*, MamY is a membrane-bound protein that aligns magnetosomes and the motility axis of helical magnetotactic bacteria. *Nat. Microbiol.* **4**, 1978–1989 (2019).
19. E. Cornejo, P. Subramanian, Z. Li, G. J. Jensen, A. Komeili, Dynamic remodeling of the magnetosome membrane is triggered by the initiation of biomineralization. *mBio* **7**, e01898-15 (2016).
20. A. Quinlan, D. Murat, H. Vali, A. Komeili, The HtrA/DegP family protease MamE is a bifunctional protein with roles in magnetosome protein localization and magnetite biomineralization. *Mol. Microbiol.* **80**, 1075–1087 (2011).
21. D. M. Hershey *et al.*, Magnetite biomineralization in Magnetospirillum magneticum is regulated by a switch-like behavior in the HtrA protease MamE. *J. Biol. Chem.* **291**, 17941–17952 (2016).
22. D. M. Hershey *et al.*, MamO is a repurposed serine protease that promotes magnetite biomineralization through direct transition metal binding in magnetotactic bacteria. *PLoS Biol.* **14**, e1002402 (2016).
23. A. Yamagishi *et al.*, Control of magnetite nanocrystal morphology in magnetotactic bacteria by regulation of mms7 gene expression. *Sci. Rep.* **6**, 29785 (2016).
24. A. Arakaki, J. Webb, T. Matsunaga, A novel protein tightly bound to bacterial magnetic particles in Magnetospirillum magneticum strain AMB-1. *J. Biol. Chem.* **278**, 8745–8750 (2003).
25. A. Lohsse *et al.*, Functional analysis of the magnetosome island in Magnetospirillum gryphiswaldense: The mamAB operon is sufficient for magnetite biomineralization. *PLoS One* **6**, e25561 (2011).
26. A. Komeili, Z. Li, D. K. Newman, G. J. Jensen, Magnetosomes are cell membrane invaginations organized by the actin-like protein MamK. *Science* **311**, 242–245 (2006).
27. R. Uebe *et al.*, The cation diffusion facilitator proteins MamB and MamM of Magnetospirillum gryphiswaldense have distinct and complex functions, and are involved in magnetite biomineralization and magnetosome membrane assembly. *Mol. Microbiol.* **82**, 818–835 (2011).
28. M. Tanaka, E. Mazuyama, A. Arakaki, T. Matsunaga, MMS6 protein regulates crystal morphology during nano-sized magnetite biomineralization in vivo. *J. Biol. Chem.* **286**, 6386–6392 (2011).
29. D. Schüler, R. Uhl, E. Bäuerlein, A simple light scattering method to assay magnetism in Magnetospirillum gryphiswaldense. *FEMS Microbiol. Lett.* **132**, 139–145 (1995).
30. S. J. Yoo *et al.*, Hydrolysis of the IciA protein, an inhibitor of DNA replication initiation, by protease Do in Escherichia coli. *FEBS Lett.* **327**, 17–20 (1993).
31. T. Clausen, M. Kaiser, R. Huber, M. Ehrmann, HTRA proteases: Regulated proteolysis in protein quality control. *Nat. Rev. Mol. Cell Biol.* **12**, 152–162 (2011).
32. R. Uebe *et al.*, The dual role of MamB in magnetosome membrane assembly and magnetite biomineralization. *Mol. Microbiol.* **107**, 542–557 (2018).
33. A. Arakaki *et al.*, Comparative subcellular localization analysis of magnetosome proteins reveals a unique localization behavior of Mms6 protein onto magnetite crystals. *J. Bacteriol.* **198**, 2794–2802 (2016).
34. S. R. Jones *et al.*, Genetic and biochemical investigations of the role of MamP in redox control of iron biomineralization in Magnetospirillum magneticum. *Proc. Natl. Acad. Sci. U.S.A.* **112**, 3904–3909 (2015).